

Testing Strong Gravitational Lensing Effects of Supermassive Black Holes with String-Inspired Metric, EHT Constraints and Parameter Estimation

Amnish Vachher,^{1,*} Shafqat Ul Islam,^{2,†} and Sushant G. Ghosh^{1,2,‡}

¹*Centre for Theoretical Physics, Jamia Millia Islamia, New Delhi 110025, India*

²*Astrophysics and Cosmology Research Unit, School of Mathematics, Statistics and Computer Science, University of KwaZulu-Natal, Private Bag 54001, Durban 4000, South Africa*

We examine and compare the gravitational lensing, in the strong field limit, for the spherically symmetric string-inspired Euler-Heisenberg black holes, characterized by additional parameters Q^2 and $\alpha - \beta$, representing magnetic charge and coupling constant, respectively. Our analysis reveals a reduction in the photon sphere radius x_{ps} , critical impact parameter u_{ps} and angular position θ_∞ with increasing magnitude of Q^2 and $\alpha - \beta$. Consequently, the value of these quantities is consistently lower than that of its GR equivalents. Further, the ratio r_{mag} of the flux of the first image to all others decreases with Q^2 and $\alpha - \beta$. Unlike Schwarzschild black holes, string-inspired Euler-Heisenberg black holes have a smaller deflection angle α_D , which decreases even more as Q^2 increases. Moreover, the time delay for Sgr A* and M87* can reach up to 11.302 and 17085.1 minutes, respectively, at $Q^2 = 0.1$ and $\alpha - \beta = -1$, deviating from Schwarzschild black holes by 0.194 and 293.6 minutes which are not very significant. For Sgr A* and M87*, we determine θ_∞ to range within (23.81, 26.28) μas and (17.89, 19.78) μas respectively, with angular separations s ranging from (3.33 – 5.67) nas for Sgr A* and (2.51 – 4.26) nas for M87*. EHT bounds on the θ_{sh} of Sgr A* and M87* within the 1σ region, bound the parameters Q^2 and $\alpha - \beta$ as: for Sgr A* $0.29278 \leq Q^2 \leq 0.60778$ and for M87* $0 < Q^2 \leq 0.08473$, but in both the cases we found no bound on the parameter $\alpha - \beta$. Our investigation reveals that a significant part of the parameter space of string-inspired Euler-Heisenberg black holes, falling within the 1σ range, is consistent with findings from the Event Horizon Telescope (EHT) concerning M87* and Sgr A*. This suggests that these black holes, inspired by string theory, could be strong contenders for astrophysical black holes. We also estimate the parameters $\alpha - \beta$ and Q^2 associated with string-inspired Euler-Heisenberg black holes using the EHT observation results of Sgr A* and M87*.

PACS numbers:

I. INTRODUCTION

The validation of Einstein's general relativity (GR) has been significantly strengthened by recent observations made by the Event Horizon Telescope (EHT), which has provided remarkable insights into the shadows cast by supermassive black holes M87* [1] and the SgrA* [2]. The observations made by the EHT provide strong support for the validity of GR and offer valuable insights into the intriguing phenomenon of strong gravitational lensing. As predicted by Einstein's general relativity, gravitational lensing is a crucial tool for exploring spacetime and studying astrophysical objects, especially black holes. It has been extensively applied across various astrophysical scenarios, aiding in understanding galaxy cluster dynamics and revealing intricate structures around supermassive black holes in galactic centres. Gravitational lensing manifests as the strong gravitational pull of a black hole bends light, leading to the emergence of a distinct "black hole shadow" at its core and a luminous "photon ring" encircling it [1, 2]. This phenomenon arises directly from the profound light bending induced by the black hole's

gravity, providing a distinctive avenue for investigating gravitational effects on a grand scale.

The exploration of gravitational lensing has a rich history, dating back to the inception of General Relativity (GR) itself [3]. The study of gravitational lensing has proven to be invaluable in understanding the structure of spacetime [4–9]. From a strong-gravitational lensing perspective, light rays near black holes can curve multiple times before reaching an observer. Notably, Darwin [10] was among the first to employ gravitational lensing concepts in the context of Schwarzschild black holes and further developed [11]. Recent theoretical studies on strong-field gravitational lensing, mainly credited to Virbhadra and Ellis [12, 13], encompass discussions on the formation and position of the ring and the magnification of relativistic images around Schwarzschild black holes. Later, Frittelli, Killing, and Newman [14] provided more rigorous analytical descriptions of the lens equation and its solution, comparing their findings with those of Virbhadra and Ellis [12, 13]. They [12] found relativistic images on each side of the optical axis alongside the primary and secondary images in Schwarzschild black hole lensing. Subsequently, Bozza [15–18] and Tsukamoto [19, 20] introduced novel methods for studying strong lensing in various spherically symmetric static spacetimes. Torres [21] derived analytical expressions for the positions and magnifications of relativistic images in Reissner-Nordström black hole lensing. The strong-

*Electronic address: amnishvachher22@gmail.com

†Electronic address: shafphy@gmail.com

‡Electronic address: sghosh2@jmi.ac.in

field gravitational lensing by black holes is also used as a means to test the predictions of general relativity [12, 14–16, 18, 19, 21–25]. Notably, numerical methods developed by Virbhadra and Ellis [12], along with analytical approaches by Bozza [15, 16, 18, 22] and Tsukamoto [19], have significantly contributed to our understanding of strong-field gravitational lensing. These methods have gained general acceptance in the scientific community and are frequently applied to investigate strong-gravitational lensing by black hole in modified gravity theories [26–40]. The strong gravitational field remains a focal point of research, with recent works exploring lensing effects from miscellaneous black holes [41–44] and modifications to Schwarzschild geometry [38, 45–50], including in the higher curvature gravity [51–53]. In particular, strong-gravitational lensing near black holes and compact objects unveils phenomena such as shadows, photon rings, and relativistic images [15, 16, 18, 22, 54–57].

The strong field gravitational lensing effects caused by a charged black hole within the framework of heterotic string theory (GHS black holes)[58, 59] was performed by Bhadra [60] and compared with the Reissner-Nordström black hole. Their findings suggested that no notable string-related influences were observed in the gravitational lensing characteristics under conditions of strong gravitational fields. Sharif and Iftikhar [61] studied the strong-gravitational lensing of charged black holes in string theory and emphasized the significant influence of the charge parameter. In the low-energy limit of string theory, Younes *et al.* [62] investigated the gravitational lensing and shadow of charged black holes. They found that the dilaton parameter significantly increases the size of the black hole shadow and the position of the innermost image. Molla *et al.* [63] examined the gravitational lensing behaviour of spherically symmetric α -corrected Reissner-Nordström black holes derived from heterotic superstring effective field theory compactified on T^6 . The parameter α acts as a correction term for the Reissner-Nordström black hole, representing the Regge slope parameter within the effective action of the heterotic superstring, as discussed in Cano *et al.* [64]. Their analysis uncovers significant distinctions compared to Reissner-Nordström’s black hole case [63].

Inspired by the aforementioned context, this study focuses on the gravitational lensing phenomena produced by the string-inspired Euler-Heisenberg black holes [65] and compares and contrasts these phenomena with those predicted by the GHS black holes [60] and the Schwarzschild black holes [16]. Furthermore, by considering supermassive black holes such as Sgr A* and M87* as the gravitational lens, we analyze the positions, separations, magnifications, and time delays in forming relativistic images. Specifically, we examine how the parameter $\alpha - \beta$ affects various gravitational lensing observables and the time delay observed between relativistic images. In addition to investigating the impact of the black hole charge Q , we also intend to explore the influence of the

parameter $\alpha - \beta$ on black hole lensing characteristics.

The paper is organized as follows: The spacetime structure of String-inspired Euler-Heisenberg Black holes is briefly reviewed for completeness, with a particular focus on the parameter space and black hole horizons in Sec. II. The framework for gravitational lensing, which encompasses the lens equation, deflection angle, and coefficients for strong lensing, is outlined in Sec. III. We analyze strong-gravitational lensing observables in Section IV, which include the position of the innermost image (θ_∞), the separation between images (s), the flux ratio of the first image to all others (r_{mag}), and the time delay between the first and second images for supermassive black holes such as Sgr A* and M87* acting as lenses. Section V focuses on constraining and estimating parameters for the string-inspired Euler-Heisenberg black hole using observational data from EHT regarding the angular shadow diameter of Sgr A* and M87*.

We conclude our findings in Section VI, wrapping up the paper. We have employed units where the speed of light and the gravitational constant are set to $8\pi G = c = 1$; however, these values are reinstated in the tables.

II. STRING-INSPIRED EULER-HEISENBERG BLACK HOLES

Here, we briefly reviewed the String-inspired Euler-Heisenberg black holes the metric, which is constructed as a modification from the metric of the GHS black hole with additional parameter $\alpha - \beta$ apart from mass M and charge Q . Here, we start with a string-loop corrected effective action, which, in the Einstein frame, is given by

$$\mathcal{S} = \frac{1}{16\pi} \int d^4x \sqrt{-g} \left[\mathcal{R} - 2\nabla^\mu \phi \nabla_\mu \phi - e^{-2\phi} \mathcal{F}^2 - f(\phi) (2\alpha \mathcal{F}_\beta^\alpha \mathcal{F}_\gamma^\beta \mathcal{F}_\delta^\gamma \mathcal{F}_\alpha^\delta - \beta \mathcal{F}^4) \right]. \quad (1)$$

It is the simplified version of the Einstein-frame action functional, resulting from a non-diagonal reduction of the Gauss-Bonnet action [66]. An exact solution within this framework is the GMGHS or GHS black hole [58, 59] when $f(\phi) = 0$. In the provided action (1), key components include \mathcal{R} representing the Ricci scalar, $\mathcal{F}^2 \equiv \mathcal{F}_{\mu\nu} \mathcal{F}^{\mu\nu} \sim E^2 - B^2$ as the Faraday scalar, and $\mathcal{F}^4 \equiv \mathcal{F}_{\mu\nu} \mathcal{F}^{\mu\nu} \mathcal{F}_{\alpha\beta} \mathcal{F}^{\alpha\beta}$, where $\mathcal{F}_{\mu\nu}$ denotes the field strength $\mathcal{F}_{\mu\nu} = \partial_\mu A_\nu - \partial_\nu A_\mu$, and α, β are coupling constants with dimensions of (length)², treated phenomenologically. The scalar field ϕ and the associated scalar function $f(\phi)$ are dimensionless. The field equations emanating from (1) are of the following form

$$G_{\mu\nu} = 2\partial_\mu \phi \partial_\nu \phi - g_{\mu\nu} \partial^\alpha \phi \partial_\alpha \phi + 2e^{-2\phi} (\mathcal{F}_\mu^\alpha \mathcal{F}_{\nu\alpha} - \frac{1}{4} g_{\mu\nu} \mathcal{F}^2) + f(\phi) (8\alpha \mathcal{F}_\mu^\alpha \mathcal{F}_\nu^\beta \mathcal{F}_\alpha^\eta \mathcal{F}_{\beta\eta} - \alpha g_{\mu\nu} \mathcal{F}_\beta^\alpha \mathcal{F}_\gamma^\beta \mathcal{F}_\delta^\gamma \mathcal{F}_\alpha^\delta r - 4\beta \mathcal{F}_\mu^\xi \mathcal{F}_{\nu\xi} \mathcal{F}^2 + \frac{1}{2} g_{\mu\nu} \beta \mathcal{F}^4), \quad (2)$$

$$4\Box\phi = -2e^{-2\phi}\mathcal{F}^2 + \frac{df(\phi)}{d\phi} (2\alpha\mathcal{F}^\alpha_\beta\mathcal{F}^\beta_\gamma\mathcal{F}^\gamma_\delta\mathcal{F}^\delta_\alpha - \beta\mathcal{F}^4) , \quad (3)$$

$$\partial_\mu \left\{ \sqrt{-g} \left[4\mathcal{F}^{\mu\nu} (2\beta f(\phi)\mathcal{F}^2 - e^{-2\phi}) - 16\alpha\mathcal{F}^\mu_\kappa\mathcal{F}^\kappa_\lambda\mathcal{F}^{\nu\lambda} \right] \right\} = 0 \quad (4)$$

By incorporating the higher-order electromagnetic invariants \mathcal{F}^4 and $\mathcal{F}^\alpha_\beta\mathcal{F}^\beta_\gamma\mathcal{F}^\gamma_\delta\mathcal{F}^\delta_\alpha$, we aim to expand upon the GMGHS solution [58, 59]. It involves introducing the general spherically symmetric metric ansatz, which can be rewritten as

$$ds^2 = -F(r)dT^2 + \frac{dr^2}{F(r)} + [R(r)]^2(d\theta^2 + \sin^2\theta d\varphi^2), \quad (5)$$

The functions $F(r)$ and $R(r)$ are unspecified and will be determined using the field equations. We also include electric and magnetic charges using the compatible spherical symmetric four-vector: $\mathcal{A}_\mu = (V(r), 0, 0, Q \cos\theta)$ with Q representing the magnetic charge. This choice of \mathcal{A}_μ satisfies the φ component of the Maxwell equations, assuming that the scalar field ϕ only depends on r . The values of the coupling constants α and β determine whether the contribution of the non-linear electromagnetic terms is significant. When $\alpha = \beta$, the higher-order electromagnetic term has no effect; however, for $\alpha \neq \beta$, the behaviour of the non-linear electromagnetic terms depends on the signs of α and β : they can either attract or repel.

$$2\alpha\mathcal{F}^\alpha_\beta\mathcal{F}^\beta_\gamma\mathcal{F}^\gamma_\delta\mathcal{F}^\delta_\alpha - \beta\mathcal{F}^4 = \frac{4(\alpha - \beta)Q^4}{[R(r)]^8} + \frac{8\beta Q^2[V'(r)]^2}{[R(r)]^4} + 4(\alpha - \beta)[V'(r)]^4 ,$$

where the prime notation signifies differentiation for r . Let's consider a non-trivial coupling function $f(\phi)$

$$f(\phi) = -[3 \cosh(2\phi) + 2] \equiv -\frac{1}{2} (3e^{-2\phi} + 3e^{2\phi} + 4) . \quad (6)$$

The coupling function $f(\phi)$ includes the dilatonic coupling $e^{2\xi\phi}$ with $\xi = \pm 1$ and a constant term. The exponential dilaton terms in the coupling function (6) can be expressed as $f(\phi) = -\frac{3}{2}(g_s^{-2} + g_s^2) - 2$, where $g_s = \exp(\phi)$ represents the string coupling, g_s^{-2} which is tree-level dilaton-Maxwell term coupling [67–69], and g_s^2 denotes corrections from two-string-loop. To find a solution to the field equations (1), taking into account (6), an exact solution for a magnetically charged black hole is given by [65] - namely String-inspired Euler-Heisenberg black holes as

$$F(r) = 1 - \frac{2M}{r} - \frac{2(\alpha - \beta)Q^4}{r^3 \left(r - \frac{Q^2}{M}\right)^3}, \quad (7)$$

$$[R(r)]^2 = r \left(r - \frac{Q^2}{M}\right). \quad (8)$$

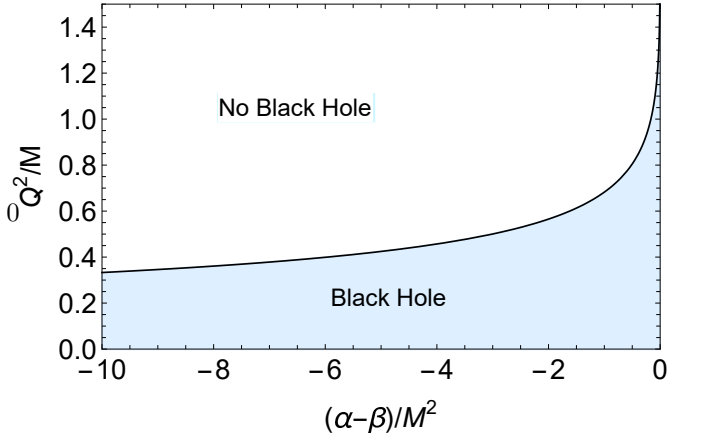


FIG. 1: The parameter space $[(\alpha - \beta)/M^2, Q^2/M]$ for the string-inspired Euler-Heisenberg black holes. The solid line separates the black hole region from the no-black hole region.

It is noteworthy that when $\alpha = \beta$, the metric (5) contains the GHS solution [58, 59] and the Schwarzschild solution [70] when $Q^2 = 0$. Note that when the radial coordinate $r \in (Q^2/M, +\infty)$, then $R \in (0, +\infty)$. The sign of coupling constants $\alpha - \beta$ is also important in determining the contribution of the higher-order electromagnetic terms. The parameter space $[(\alpha - \beta)/M^2, Q^2/M]$ for the string-inspired Euler-Heisenberg black holes is illustrated in Fig. 1. The solid line separating the black hole region from the no-black hole region corresponds to an extremal string-inspired Euler-Heisenberg BH with degenerate horizons. The light blue (black hole) region corresponds to the values of parameters as $Q^2 \in (0, 2)$ and $(\alpha - \beta) \in (-\infty, 0)$.

For the discussion on gravitational lensing, we rewrite the metric (5) by redefining the following quantities $r, T, \alpha - \beta, Q^2$ in the unit of M as

$$d\bar{s}^2 = -A(x)dt^2 + \frac{1}{A(x)}dx^2 + C(x)d\Omega^2, \quad (9)$$

$$A(x) = 1 - \frac{2}{x} + \frac{2(\alpha - \beta)Q^4}{x^3(x - Q^2)^3}, \quad (10)$$

$$C(x) = x(x - Q^2),$$

The horizons of the string-inspired Euler-Heisenberg black holes can be obtained from $g^{rr} = A(x) = 0$, that is

$$A(x) = 1 - \frac{2}{x} + \frac{2(\alpha - \beta)Q^4}{x^3(x - Q^2)^3} = 0. \quad (11)$$

The elementary analysis of $A(x) = 0$ suggests that, depending on the values of parameters Q^2 and $\alpha - \beta$, $A(x)$ admits up to two real positive roots. The sign of $\alpha - \beta$ for coupling constants decides whether the black holes have two horizons (for $(\alpha - \beta) < 0$) or one horizon (for $(\alpha - \beta) > 0$) [65]. The event horizon (x_+) decreases slowly with the parameter Q^2 increasing. Still, the Cauchy horizon (x_-) increases rapidly with increasing Q^2 and at

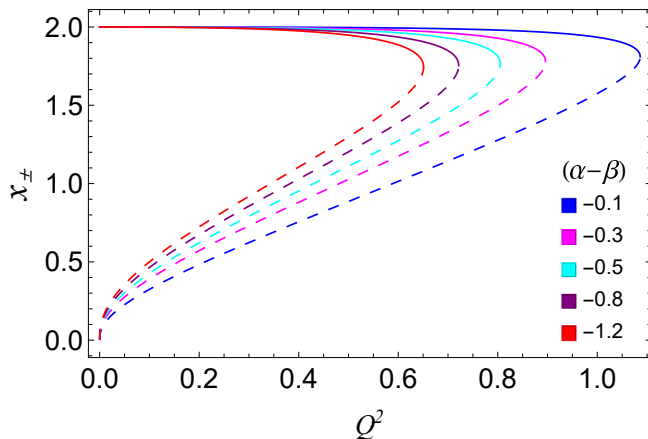


FIG. 2: Position of the event horizon (x_+) represented by solid lines and Cauchy horizon (x_-) represented by dashed lines for string-inspired Euler-Heisenberg black holes along with parameter Q^2 at different values of the parameter $\alpha - \beta$.

a certain value, it merges with the event horizon. (c.f. Fig. 2).

III. STRONG GRAVITATIONAL LENSING BY BLACK HOLE

The deflection angle and lens equation govern the strong gravitational lensing by a black hole [15, 16]. The null geodesic equation satisfies the equation reads as

$$\left(\frac{dx}{d\tau}\right)^2 \equiv \dot{x}^2 = \mathcal{E}^2 - \mathcal{L}^2 \frac{A(x)}{C(x)}. \quad (12)$$

where energy $\mathcal{E} = -p_\mu \xi_t^\mu$, and angular momentum $\mathcal{L} = p_\mu \xi_\phi^\mu$ such that ξ_t^μ and ξ_ϕ^μ are killing vectors, associated with time translation symmetry and axial rotational symmetry, respectively. The path of photons orbiting around a black hole can be described by radial effective potential [71], for which the string-inspired Euler-Heisenberg black holes reads

$$V_{\text{eff}}(x) = -1 + \frac{u^2}{x(x-Q^2)} \left(1 - \frac{2}{x} - \frac{2(\alpha-\beta)Q^4}{x^3(x-Q^2)^3}\right) \quad (13)$$

For a photon to remain in a stable circular orbit, the effective potential should exhibit a local maximum, indicating a stable equilibrium point. At this maximum potential, photons can orbit the black hole at that specific radius without being drawn into it or escaping to infinity. Nevertheless, even a minor disturbance can disrupt this equilibrium, leading the photons to fall into the black hole or escape to infinity. This scenario characterizes the circular orbit as an unstable photon sphere [12, 16].

The conditions for the existence of a photon sphere around a black hole are determined by the properties of the spacetime metric, particularly the radial effective potential $V_{\text{eff}}(x)$. A light ray exists in the region

where $V_{\text{eff}} \leq 0$ (refer to Figures 3 and 4). Additionally, one can define an unstable (or stable) circular orbit that satisfies $V_{\text{eff}} = V'_{\text{eff}}(x) = 0$ and $V''_{\text{eff}}(x_{ps}) < 0$ (or $V''_{\text{eff}}(x_{ps}) > 0$). In the case of string-inspired Euler-Heisenberg black hole spacetime, we observe that $V''_{\text{eff}}(x_{ps}) < 0$, indicating unstable photon circular orbits (refer to Figures 3 and 4).

The radius of photon sphere (x_{ps}) which is the largest positive root of [13, 72] can be described by:

$$\frac{A'(x)}{A(x)} = \frac{C'(x)}{C(x)} \quad (14)$$

which is depicted in Fig. 5. The photon sphere radii x_{ps} decreases with the parameters Q^2 and $\alpha - \beta$.

By solving $V_{\text{eff}}(x_0) = 0$ we get the expression for impact parameter u in terms of the closest approach distance x_0 as [16]

$$u \equiv \left| \frac{\mathcal{L}}{\mathcal{E}} \right| = \sqrt{\frac{C(x_0)}{A(x_0)}}. \quad (15)$$

As the x_0 approaches x_{ps} the deflection angle becomes unboundedly large and the impact parameter u becomes the critical impact parameter u_{ps} [12]

The deflection angle as a function of the closest approach distance in the strong field limit can be described as [12] as

$$\alpha_D(x_0) = I(x_0) - \pi, \quad (16)$$

where

$$I(x_0) = 2 \int_{x_0}^{\infty} \frac{d\varphi}{dx} dx, \quad (17)$$

here

$$\frac{d\varphi}{dx} = \frac{1}{\sqrt{A(x)C(x)} \sqrt{(A(x_0)/C(x))(A(x)/C(x_0)) - 1}}. \quad (18)$$

Now let us define a new variable $z = 1 - x_0/x$ [73, 74]. Using this, we can rewrite the Eq. 17 as

$$I(x_0) = \int_0^1 R(z, x_0) f(z, x_0) dz. \quad (19)$$

such that $R(z, x_0)$ is

$$R(z, x_0) = \frac{2x_0}{(1-z)^2} \frac{\sqrt{C(x_0)}}{C(x)}, \quad (20)$$

and $f(z, x_0)$ as

$$f(z, x_0) = \frac{1}{\sqrt{A(x_0) - A(x) \frac{C(x_0)}{C(x)}}}. \quad (21)$$

where $R(z, x_0)$ is regular, but the function $f(z, x_0)$ diverges when $z = 0$. Therefore, to avoid the divergence,

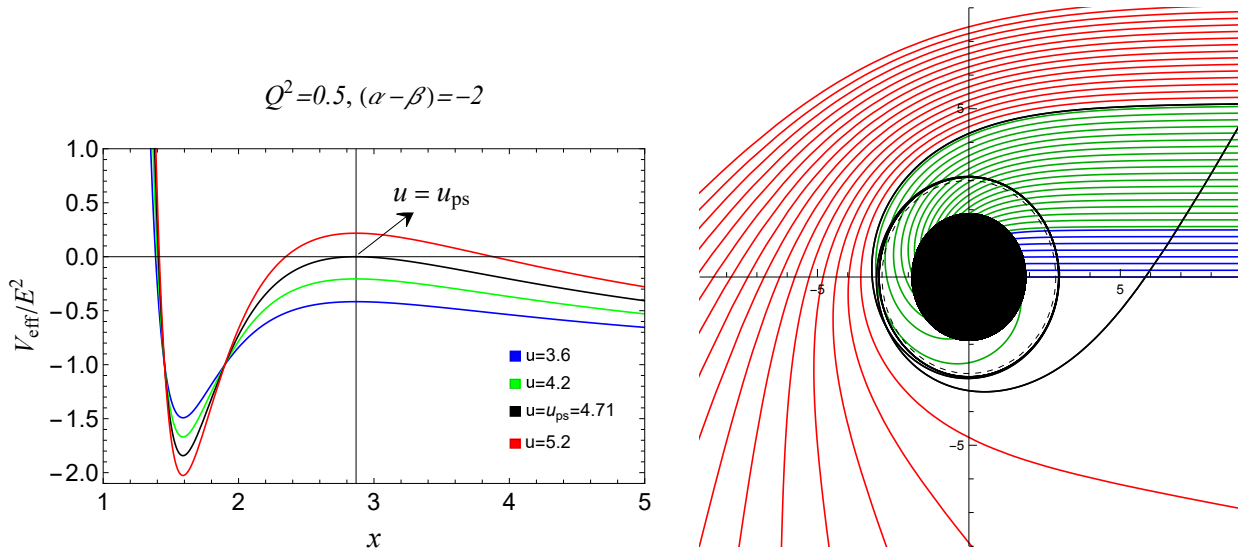


FIG. 3: Variation of the effective potential V_{eff} for string-inspired Euler-Heisenberg black holes at $Q^2 = 0.5$ and $\alpha - \beta = -2$ with radial coordinate x . The photons with black solid lines make unstable circular orbits around black holes with critical impact parameters (u_{ps}) (left). The trajectory of the light ray for $Q^2 = 0.5$ and $\alpha - \beta = -2$, for different impact parameters u in polar coordinates (r, ϕ) . The black line corresponds to the $u \approx u_{ps}$ value. Note that here we have shown the black hole as a solid disk and the unstable photon sphere as a dashed black circle (right).

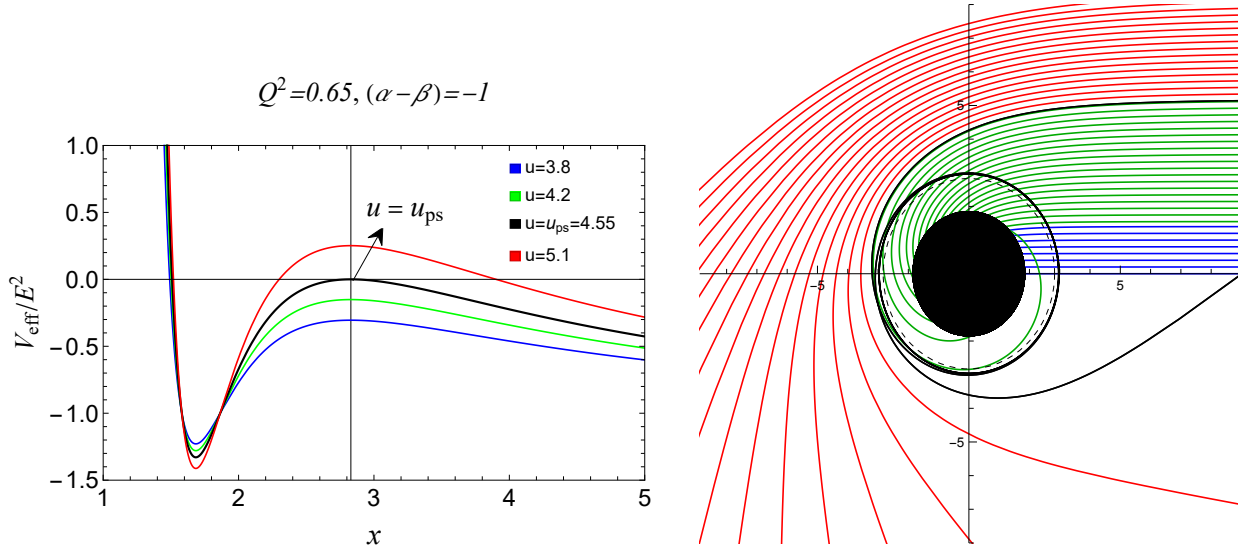


FIG. 4: Variation of the effective potential V_{eff} for string-inspired Euler-Heisenberg black holes at $Q^2 = 0.65$ and $\alpha - \beta = -1$ with radial coordinate x . The photons with black solid lines make unstable circular orbits around black holes with critical impact parameters (u_{ps}) (left). The trajectory of the light ray for $Q^2 = 0.65$ and $\alpha - \beta = -1$, for different impact parameters u in polar coordinates (r, ϕ) . The black line corresponds to the $u \approx u_{ps}$ value. We have shown the black hole as a solid disk and the unstable photon sphere as a dashed black circle (right).

we do a Taylor series expansion for $f(z, x_0)$ at $z = 0$ to approximate the function $f(z, x_0) \approx f_0(z, x_0)$

$$f_0(z, x_0) = \frac{1}{\sqrt{\Gamma(x_0)z + \gamma(x_0)z^2}}, \quad (22)$$

Now, the integral can be divided into two parts as

$$I(x_0) = I_D(x_0) + I_R(x_0), \quad (23)$$

where $I_D(x_0)$ is the divergent part described as

$$I_D(x_0) = \int_0^1 R(0, x_{ps}) f_0(z, x_0) dz, \quad (24)$$

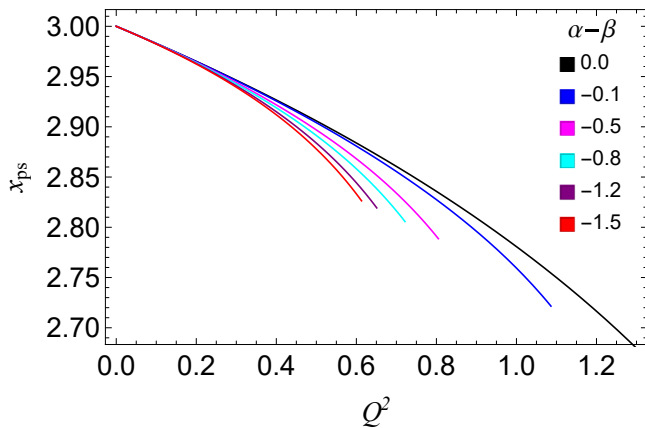


FIG. 5: The photon sphere radius (x_{ps}) along with parameter Q^2 for different values of parameter $\alpha - \beta$. The black solid line corresponds to the GHS black holes.

and $I_R(x_0)$ is the regular part

$$I_R(x_0) = \int_0^1 g(z, x_0) dz, \quad (25)$$

$$g(z, x_0) = R(z, x_0)f(z, x_0) - R(0, x_{ps})f_0(z, x_0)$$

By solving both the integrals (24) and (25), the deflection angle as a function of impact parameter u which can be written in terms of angular position of image as $u \approx \theta_{DOL}$, near $u \rightarrow u_{ps}$ can be described as [16, 75]

$$\alpha_D(u) = -\bar{a} \log\left(\frac{u}{u_{ps}} - 1\right) + \bar{b} + O(u - u_{ps}). \quad (26)$$

where \bar{a} and \bar{b} are the strong lensing coefficients described as

$$\bar{a} = \frac{R(0, x_{ps})}{2\sqrt{\gamma(x_{ps})}}, \quad (27)$$

$$\bar{b} = -\pi + I_R(x_{ps}) + \bar{a} \log\left(\frac{2\gamma(x_{ps})}{A(x_{ps})}\right). \quad (28)$$

We have characterized the relationship between the strong gravitational lensing coefficients and parameters of string-inspired Euler-Heisenberg BH through numerical methods. The deflection coefficient \bar{a} gradually increases with parameter Q^2 and the $(\alpha - \beta)$ magnitude. In contrast, the deflection coefficient \bar{b} gradually decreases as parameters Q^2 as well as with $(\alpha - \beta)$ (see Table III). The critical impact parameter also gradually decreases as the parameter Q^2 increases and parameter $\alpha - \beta$ decreases (see Table III). Note when the parameters Q^2 and $\alpha - \beta$ vanish, the string-inspired Euler-Heisenberg black hole becomes Schwarzschild BH, such that $\bar{a} = 1$, $\bar{b} = -0.40023$ (see Table III). Also, parameters $Q^2 \neq 0$ and $\alpha = \beta$ correspond to GHS black holes (see Table III). Figure 6, illustrates that the deflection angle diverges at specific impact parameter values $u = u_{ps}$ for

different Q^2 . The deflection angle of the string-inspired Euler-Heisenberg black hole gradually decreases as the parameter Q^2 increases for the fixed value of parameter $\alpha - \beta$ (cf. Fig. 6).

Q^2	$(\alpha - \beta)$	\bar{a}	\bar{b}	u_{ps}/R_s
0.0	0.0	1.00	-0.40023	5.19615
	0.0	1.0057	-0.40828	5.1085
0.1	-0.1	1.00577	-0.40828	5.10854
	-0.5	1.00603	-0.40829	5.10844
	-1	1.00635	-0.40829	5.10832
	-2	1.00701	-0.40831	5.10808
0.3	0.0	1.0181	-0.4269	4.9269
	-0.1	1.01894	-0.42702	4.9267
	-0.5	1.02237	-0.42721	4.92553
	-1	1.02673	-0.42748	4.92407
0.5	-2	1.03569	-0.42811	4.9211
	0.0	1.0321	-0.45005	4.7356
	-0.1	1.03574	-0.45037	4.73453
	-0.5	1.05068	-0.45188	4.73002
	-1	1.07076	-0.4544	4.72426
	-2	1.1165	-0.46218	4.71229

TABLE I: Strong lensing coefficients \bar{a} and \bar{b} and critical impact parameter u_{ps} for different values of parameter of string-inspired Euler-Heisenberg black holes are presented in the table. Note that $\alpha - \beta = 0$ and $Q^2 \neq 0$ correspond to GHS Black holes.

IV. STRONG GRAVITATIONAL LENSING EFFECT FOR SUPERMASSIVE BLACK HOLES

A. Strong lensing Observables

In the previous section III, we calculated the deflection angle for strong gravitational lensing; now assuming that the source and observer are far from the black hole, we deduce that asymptotically flat lens equation as [12, 15]

$$\psi = \theta - \frac{D_{LS}}{D_{OS}} \Delta\alpha_n, \quad (29)$$

where D_{LS} is the distance between the lens and the light source, and D_{OS} is the distance between the observer and the light source. Also, the angular positions of the source and image are ψ and θ , respectively, and $\Delta\alpha_n = \alpha(\theta) - 2n\pi$ is the offset of deflection, where n is the integer represents the number of loops. For the position of the n th relativistic image, we solve Eq. 29 with Eq. 28 [16].

$$\theta_n = \theta_n^0 + \frac{u_{ps} e_n (\psi - \theta_n^0) D_{OS}}{\bar{a} D_{LS} D_{OL}}. \quad (30)$$

where

$$e_n = \exp\left(\frac{\bar{b} - 2n\pi}{\bar{a}}\right). \quad (31)$$

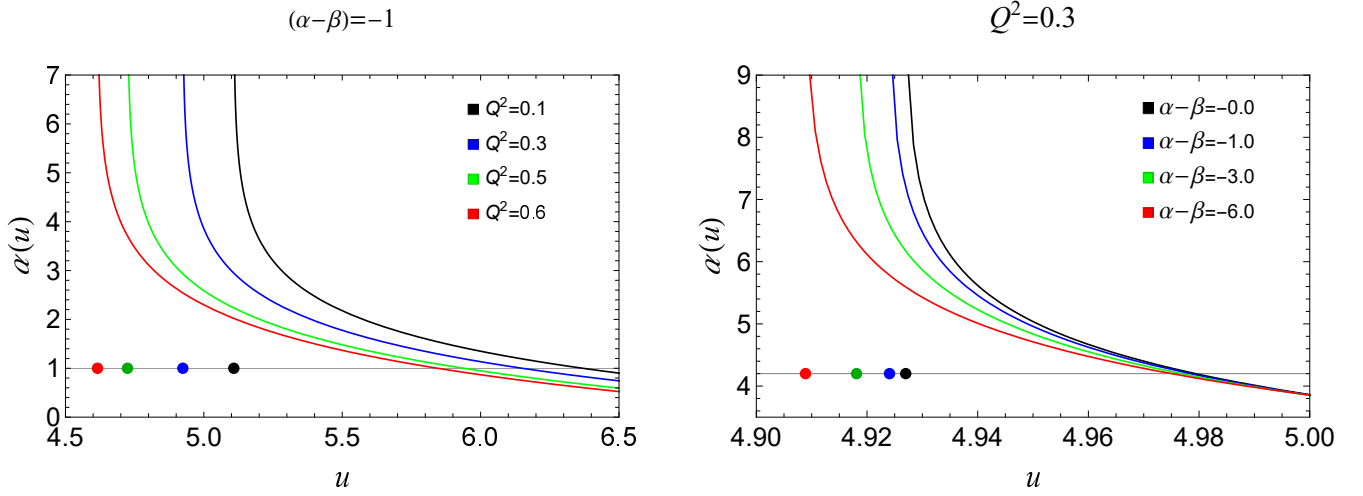


FIG. 6: Variation of deflection angle as a function of impact parameter u for different values of parameters Q^2 (left) and $\alpha - \beta$ (right) keeping the values one of the parameter as constant for String-inspired Euler-Heisenberg black holes. Points on the horizontal line represent the values of the critical impact parameter u_{ps} at which the deflection angle diverges. Note that the black solid line in the right figure for which $Q^2 = 0.3$ and $\alpha - \beta = 0$ corresponds to the GHS BH.

where θ_n^0 correspond to the image position at $\alpha = 2n\pi$. From equation 30, we see that when $\psi = \theta_n^0$, then the position of the image coincides with the source. At this moment, the position of the image $\theta_n = \theta_n^0$, representing that the source and the image are on the same side. However, to locate the n th image on the opposite side of the source, this condition is extended by substituting ψ with $-\psi$, thereby determining the image's position across the source.

The n th relativistic image magnification can be defined as [16, 24, 76]

$$\mu_n = \left(\frac{\psi}{\theta} \frac{d\psi}{d\theta} \right)^{-1} \Big|_{\theta_n^0} = \frac{u_{ps}^2 e_n (1 + e_n) D_{OS}}{\bar{a} \psi D_{LS} D_{OL}^2}, \quad (32)$$

where the first relativistic image is the brightest, and the magnification decreases exponentially with increasing n . Since the magnification is inversely proportional to the square of the distance between the observer and the lens thus, the relativistic images are very faint. When $\psi \rightarrow 0$, i.e., perfect alignment, we have the Einstein ring.

We now calculate the three lensing observables to analyze the strong-gravitational lensing phenomena. Here, we consider the outermost image as θ_1 and all the other inner packed images as θ_∞ [16]. The angular position of the asymptotic relativistic image θ_∞ ,

$$\theta_\infty = \frac{u_{ps}}{D_{OL}}, \quad (33)$$

the angular separation s between the outermost and all the other packed images is

$$s \equiv \theta_1 - \theta_\infty = \theta_\infty \exp\left(\frac{\bar{b} - 2\pi}{\bar{a}}\right), \quad (34)$$

the flux ratio of the brightness flux between the outermost image θ_1 and the remaining relativistic images at θ_∞ is

$$r = \frac{\mu_1}{\sum_{n=2}^{\infty} \mu_n} = 2.5 \log_{10} \left[\exp\left(\frac{2\pi}{\bar{a}}\right) \right], \quad (35)$$

Note that the flux ratio is independent of the distance between the lens and the observer D_{OL} . We can obtain the coefficients \bar{a} , \bar{b} and the critical impact parameter u_{ps} , using the three lensing observables defined above to analyze the properties specific to string-inspired Euler-Heisenberg black holes. By comparing astronomical observations with analyzed data, we can comprehensively understand the properties and behaviour of string-inspired Euler-Heisenberg black holes.

B. Strong Lensing effect for the supermassive black holes M87* and Sgr A*

We use string-inspired Euler-Heisenberg black holes to estimate the lensing observables of the supermassive black holes M87* and Sgr A* and compare our data with that of Schwarzschild and GHS black holes. Based on the latest astronomical observation data, the estimated mass of M87* is $(6.5 \pm 0.7) \times 10^9 M_\odot$, and its distance is $d = 16.8 \text{ Mpc}$ [77]. The estimated mass of Sgr A* is $4_{-0.6}^{+1.1} \times 10^6 M_\odot$, and its distance is $d = 7.97 \text{ kpc}$ [78].

When the black hole is perfectly aligned ($\psi \approx 0$) with the observer and the lens and is at the centre of the observer and the light source, such that $D_{OS} = D_{LS} = 2D_{OL}$ [11], then equation (30) will yield [79]

$$\theta_n^E = \left(1 - \frac{u_{ps} e_n D_{OS}}{\bar{a} D_{LS} D_{OL}} \right) \theta_n^0. \quad (36)$$

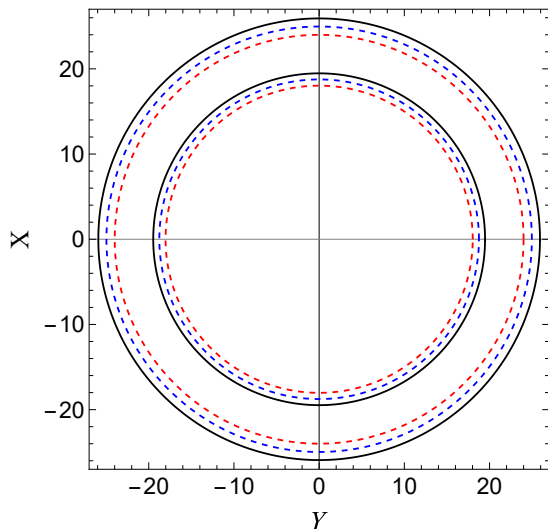


FIG. 7: Einstein rings for supermassive black holes when considering them as string-inspired Euler-Heisenberg black holes. Outer rings correspond to Sgr A*, and Inner rings correspond to M87* at the values $Q^2 = 0.1$ and $\alpha - \beta = -1$ (black solid line) and $Q^2 = 0.5$ and $\alpha - \beta = -0.8$ (red dashed line). The blue dashed line represents the GHS black holes ($\alpha - \beta = 0$ and $Q^2 = 0.3$).

where θ_n^E is the Einstein ring [4]. Now assuming that the distance D_{OL} is greater than the impact parameter i.e. $u_{ps}(D_{OL} \gg u_{ps})$, then 36 becomes

$$\theta_n^E \approx \frac{u_{ps}(1 + e_n)}{D_{OL}}, \quad (37)$$

At $n = 1$, the outermost ring is formed, and the radius of the ring decreases with increases in the value of n . The outermost relativistic Einstein ring of M87* and SgrA* are shown in Figure 7. When the parameter Q^2 increases, the Einstein ring becomes smaller for Sgr A* and M87*. Clearly, as shown in Fi. 9 and Table III, the image position θ_∞ and the relativistic image brightness ratio r_{mag} decreases with increasing magnitude of the parameters Q^2 as well as $(\alpha - \beta)$ (cf. Fig. 8) and the image separation s to increases with increase in parameter Q^2 and $(\alpha - \beta)$ (cf. Fig. 9). It is noteworthy that in both M87* and SgrA*, the variation of the angular position of the relativistic images along with parameters ranges from $19.78\mu as \geq \theta_\infty \geq 17.89\mu as$ for M87* and $26.28\mu as \geq \theta_\infty \geq 23.81\mu as$ for Sgr A*. From Table III and Figure 9 we see that the deviation in the angular position of the relativistic images θ_∞ and the angular separation s between the string-inspired Euler-Heisenberg black holes and its GR counterpart is not very large (around $1\mu as$). We have also compared the lensing observables of string-inspired Euler-Heisenberg black holes with the case where $\alpha = \beta$, i.e. GHS black hole (see Figure 9 and Table III).

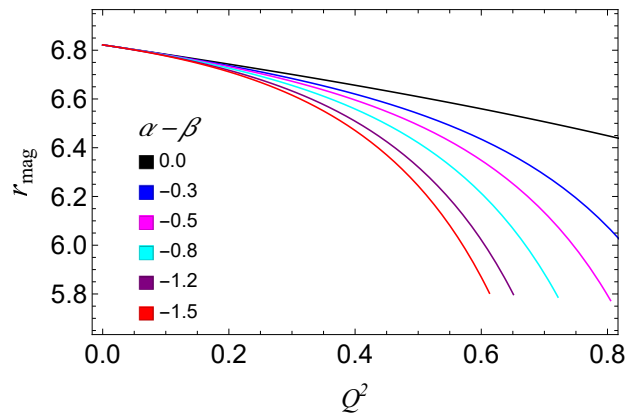


FIG. 8: Variation of strong lensing observable r_{mag} for string-inspired Euler-Heisenberg black hole with parameter Q^2 for different values of parameters $\alpha - \beta$. Note that r_{mag} is independent of the black hole's mass or distance from the observer.

C. Estimation of Time Delay for SMBHs

Time delay between different images occurs due to the different paths taken by the photon while winding the black hole. By assuming the source to be variable, we can numerically calculate the time delay between different relativistic images. To calculate the time delay, we first calculate the total time period of photon to travel from source to the observer [75]

$$T = \tilde{T}(x_0) - \int_{D_{OL}}^{\infty} \left| \frac{dt}{dx} \right| dx - \int_{D_{LS}}^{\infty} \left| \frac{dt}{dx} \right| dx, \quad (38)$$

When the source and the observer are far from the black hole, then the second and third terms on the right-hand side cancel each other, then the total time is written as

$$\tilde{T}(x_0) = \int_{x_0}^{\infty} \frac{2\sqrt{C(x)A(x_0)}}{A(x)\sqrt{A(x)}\sqrt{\frac{C(x)}{C(x_0)}\frac{A(x_0)}{A(x)} - 1}} dx, \quad (39)$$

The integral $\tilde{T}(x_0)$ represents when the photon winds around the black hole. In the strong deflection limit, the total time can be expanded as a function of u as

$$\tilde{T}(u) = -\tilde{a} \log\left(\frac{u}{u_{ps}} - 1\right) + \tilde{b} + \mathcal{O}(u - u_{ps}), \quad (40)$$

where \tilde{a} and \tilde{b} are strong deflection limit coefficients and $\tilde{a} = \tilde{a}u_{ps}$ for the spacetime (11) [75].

For spherically symmetric black holes, we can distinguish the case when the two images are on the same side of the lens from the case or when the two images are on opposite sides.

If we can at least distinguish the time signals of the outermost relativistic image from those of the second image, then the time delay between the first and the second relativistic image $\Delta T_{2,1}$ can be calculated by strong deflection limit coefficients as [75]

$$\Delta T_{2,1}^s = 2\pi u_{ps} = 2\pi D_{OL}\theta_\infty, \quad (41)$$

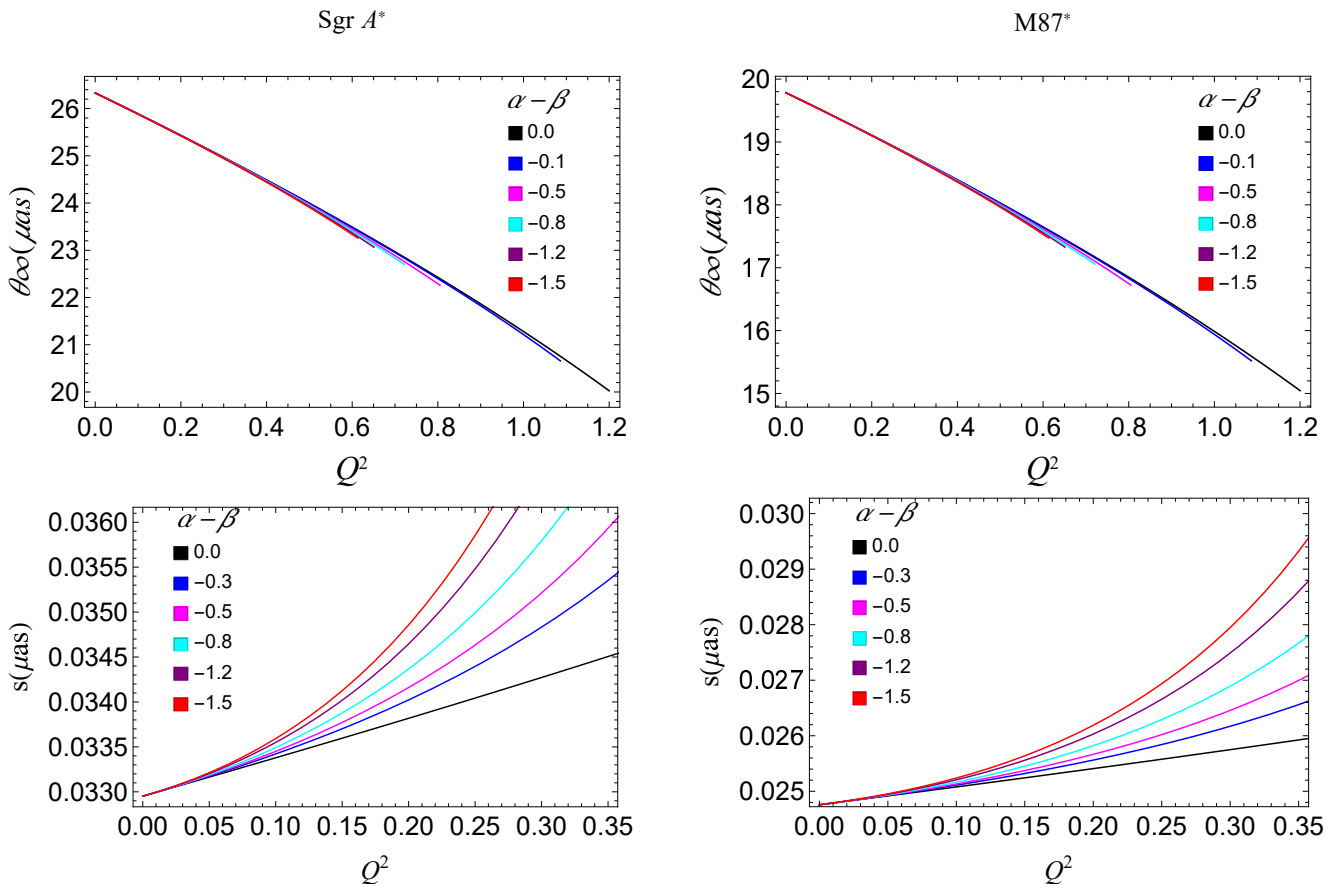


FIG. 9: Variation of strong lensing observables θ_∞ (upper panel) and s (lower panel) with Q^2 for different values of $\alpha - \beta$ for Sgr A* and M87* respectively. Black solid line in these plots represent GHS black holes.

From Eq. 41, we can estimate the distance of the black hole. In Table III, we compare time delay $\Delta T_{2,1}^s$ for the supermassive black holes at the centre of different galaxies representing Schwarzschild, string-inspired Euler-Heisenberg and GHS black holes and also calculated their difference $\delta T_{12}^s = \Delta T_{2,1}^s(\text{Sch}) - \Delta T_{2,1}^s(\text{EH})$.

V. EHT CONSTRAINTS AND PARAMETER ESTIMATION

The Event Horizon Telescope (EHT) observation results have revolutionized our understanding of supermassive black holes, unveiling horizon-scale images of M87* and Sgr A*. In 2019, the EHT Collaboration's groundbreaking work confirmed the existence of black holes with the unveiling of M87*'s image, revealing an angular diameter of $\theta_d = 42 \pm 3 \mu\text{as}$ for its compact emission region, defining the central flux depression as the black hole's shadow [1, 77, 80]. Subsequent observations in 2022 captured Sgr A*, presenting a distinct ring with $\theta_d = 48.7 \pm 7 \mu\text{as}$ and quantifying the Schwarzschild shadow deviation as $\delta = -0.08_{-0.09}^{+0.09}$ (VLTI), $-0.04_{-0.10}^{+0.09}$

(Keck) [81]. Sgr A* offers a unique opportunity due to its probing of curvature orders higher than M87*, and the independent prior estimates for the mass-to-distance ratio utilized for Sgr A*. The use of three independent imaging algorithms ensures robustness, with the average diameter of the Sgr A* shadow constrained to be within $46.9 \mu\text{as} \leq \theta_{\text{sh}} \leq 50 \mu\text{as}$. The EHT result for Sgr A* also calculated the emission ring angular diameter $\theta_d = (51.8 \pm 2.3) \mu\text{as}$ [81]. These findings not only enable exploration of strong-field gravity but also offer insights into theoretical frameworks and put constraints on additional parameters within gravity theories [26, 82–89]. Leveraging the EHT data, we apply these observations to assess the feasibility of string-inspired Euler-Heisenberg black holes, placing constraints on deviation parameters Q^2 and $\alpha - \beta$. By adopting the apparent radius of the photon sphere θ_∞ as the angular measurement for the black hole shadow, constraints are established at the 1- σ confidence level. M87* and Sgr A* are modelled as string-inspired Euler-Heisenberg black holes, underpinning efforts to understand the implications of magnetically charged black holes in cosmic phenomena. This synthesis of observational data and theoretical frameworks advances our understanding of black hole physics and

Q^2	$(\alpha - \beta)$	Sgr A*		M87*		r_{mag}
		$\theta_\infty (\mu as)$	$s (\mu as)$	$\theta_\infty (\mu as)$	$s (\mu as)$	
0.0	0.0	26.33	0.03295	19.78	0.02476	6.8219
	0.0	25.886	0.03338	19.448	0.02508	6.7832
	-0.1	25.8859	0.03339	19.4485	0.02509	6.7828
0.1	-1.0	25.8848	0.03352	19.4476	0.02518	6.7788
	-4.5	25.8805	0.03402	19.4444	0.02556	6.7634
	-9.5	25.8743	0.03476	19.4397	0.02612	6.7412
	0.0	24.966	0.03427	18.757	0.02574	6.7006
	-0.1	24.9645	0.03446	18.7562	0.02589	6.6951
0.3	-1	24.9511	0.03619	18.7462	0.02719	6.6443
	-2.5	24.9286	0.03934	18.7292	0.02955	6.5575
	-4.5	24.8978	0.04413	18.7061	0.03316	6.4375
	0.0	23.996	0.03523	18.028	0.02647	6.6094
	-0.1	23.9908	0.03602	18.0246	0.02706	6.5865
0.5	-0.5	23.9679	0.03942	18.0074	0.02962	6.4928
	-1	23.9387	0.04429	17.9855	0.03328	6.3711
	-2	23.878	0.05678	17.9399	0.04266	6.1101

TABLE II: Estimates for Strong lensing observables for the string-inspired Euler-Heisenberg black holes and compared with Schwarzschild black holes ($Q^2 \rightarrow 0, (\alpha - \beta) \rightarrow 0$) in GR considering the supermassive black holes Sgr A* and M87* as lens for different values of parameter Q^2 and $(\alpha - \beta)$. Note that $Q^2 \neq 0$ and $\alpha - \beta = 0$ correspond to GHS Black holes.

underscores the interdisciplinary nature of contemporary astrophysical research.

a. Constraints from Sgr A:* The shadow angular diameter (θ_{sh}), is averaged at a range of (46.9, 50) μas , with a 1- σ interval of the Sgr A* black hole for the EHT observation; hence it imposes constraints on the parameters of string-inspired Euler-Heisenberg black holes, Q^2 and $\alpha - \beta$ as illustrated in Fig. 10. Here θ_{sh} is depicted as a function of parameters Q^2 and $(\alpha - \beta)$, the black and black dashed line corresponds to $\theta_{sh} = 50$ and $\theta_{sh} = 46.9$ respectively. The constraints on the parameters range as $0.29278 \leq Q^2 \leq 0.60778$, but there is no constraint on the parameter value $(\alpha - \beta)$. So, within the above-defined parameter range, the string-inspired Euler-Heisenberg black hole aligns with the Sgr A* black hole shadow observations from the EHT.

b. Constraints from M87:* Fig. 11 depicts the angular diameter θ_{sh} as a function of parameters Q^2 and $\alpha - \beta$, with the black solid line corresponding to $\theta_{sh} = 39 \mu as$ for the string-inspired Euler-Heisenberg black holes as M87*. When we investigated the string-inspired Euler-Heisenberg black holes with the EHT results of M87* within the 1- σ bound, it constrains the parameters Q^2 and $\alpha - \beta$, viz., $0 < Q^2 \leq 0.08473$ but there is no constraint on the value of the parameter $(\alpha - \beta)$. Thus, based on Fig. 11, a string-inspired Euler-Heisenberg black hole can be a candidate for astrophysical black holes.

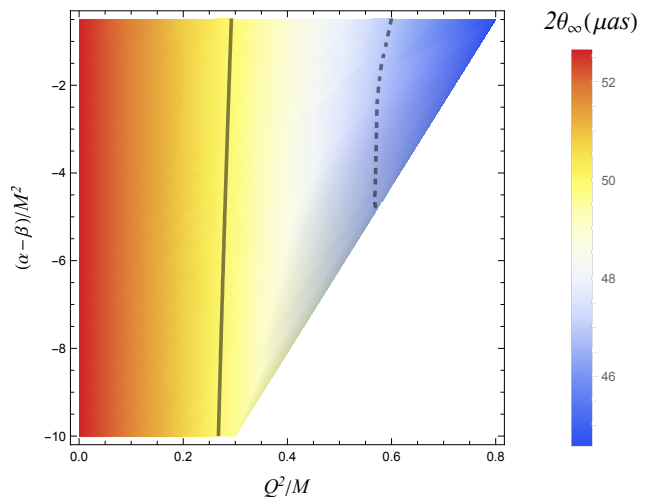


FIG. 10: Shadow angular diameter $\theta_{sh}(= 2\theta_\infty)$ as a function of parameters Q^2 and $(\alpha - \beta)$, when Sgr A* is modelled as string-inspired Euler-Heisenberg BH. The black and black dashed line corresponds to $\theta_{sh} = 50$ and $\theta_{sh} = 46.9$ respectively. The region between these lines satisfies the Sgr A* shadow 1- σ bound.

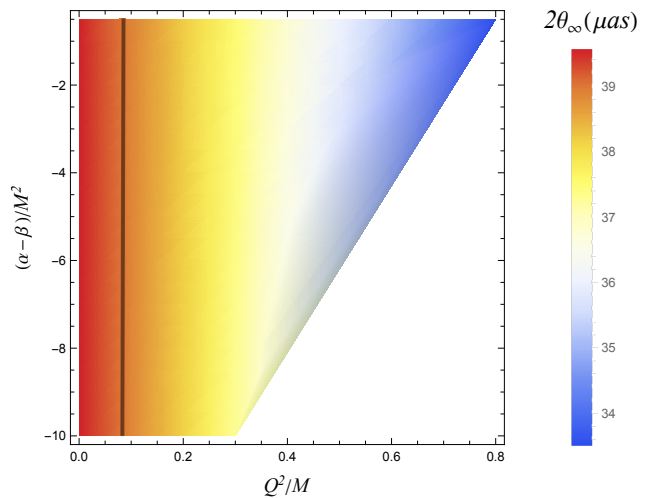


FIG. 11: Shadow angular diameter $\theta_{sh}(= 2\theta_\infty)$ as a function of parameters Q^2 and $(\alpha - \beta)$, when M87* is modelled as string-inspired Euler-Heisenberg BH. The black line corresponds to $\theta_{sh} = 39$. The region within this line satisfies the M87* shadow 1- σ bound.

A. Estimation of Black holes Parameters

By analyzing the angular shadow diameter of supermassive black holes like M87* and Sgr A* using data from the Event Horizon Telescope (EHT), we have estimated the parameters associated with the string-inspired Euler-Heisenberg model [89–91]. This estimation of black hole parameters helps us understand the implications of magnetic charge and string coupling constants on these astrophysical objects.

In Table. IV and V, we estimate the parameters Q^2

TABLE III: Time delay estimation between the first and second relativistic image $\Delta T_{2,1}^s$ for different supermassive black holes at the centre of nearby galaxies considering string-inspired Euler-Heisenberg black hole ($Q^2 = 0.1$ and $\alpha - \beta = -1$) and GHS black holes ($Q^2 = 0.1$ and $\alpha - \beta = 0$) in comparison with Schwarzschild ($Q^2 \rightarrow 0$ and $\alpha - \beta \rightarrow 0$). Note that time delays are calculated in minutes and $\delta T_{12}^1 = \Delta T_{2,1}^s(Sch) - \Delta T_{2,1}^s(EH)$ and $\delta T_{12}^2 = \Delta T_{2,1}^s(Sch) - \Delta T_{2,1}^s(GHS)$.

Galaxy	$M(M_\odot)$	D_{OL} (Mpc)	M/D_{OL}	ΔT_{12}^s (Sch)	ΔT_{12}^s (EH)	ΔT_{12}^s (GHS)	δT_{12}^1	δT_{12}^2
Milky Way	4.3×10^6	0.008	2.471×10^{-11}	11.4968	11.3024	11.303	0.1944	0.1938
M87	6.5×10^9	16.8	1.758×10^{-11}	17378.7	17085.1	17085.9	293.6	292.8
NGC 4472	2.54×10^9	16.72	7.246×10^{-12}	6791.06	6676.32	6676.64	114.74	114.42
NGC 1332	1.47×10^9	22.66	3.094×10^{-12}	3930.26	3863.86	3864.04	66.4	66.2
NGC 4374	9.25×10^8	18.51	2.383×10^{-12}	2473.12	2431.34	2431.45	41.78	41.67
NGC 1399	8.81×10^8	20.85	2.015×10^{-12}	2355.48	2315.68	2315.8	39.8	39.68
NGC 3379	4.16×10^8	10.70	1.854×10^{-12}	1112.24	1093.44	1093.5	18.8	18.74
NGC 4486B	6×10^8	16.26	1.760×10^{-12}	1604.19	1577.08	1577.16	27.11	27.03
NGC 1374	5.90×10^8	19.57	1.438×10^{-12}	1577.45	1550.8	1550.87	26.65	26.58
NGC 4649	4.72×10^9	16.46	1.367×10^{-12}	12619	12406.4	12407	212.6	212
NGC 3608	4.65×10^8	22.75	9.750×10^{-13}	1243.25	1222.24	1222.3	21.01	20.95
NGC 3377	1.78×10^8	10.99	7.726×10^{-13}	475.909	467.868	467.89	8.041	8.019
NGC 4697	2.02×10^8	12.54	7.684×10^{-13}	540.077	530.952	530.977	9.125	9.1
NGC 5128	5.69×10^7	3.62	7.498×10^{-13}	152.131	149.56	149.567	2.571	2.564
NGC 1316	1.69×10^8	20.95	3.848×10^{-13}	451.816	444.212	444.233	7.604	7.583
NGC 3607	1.37×10^8	22.65	2.885×10^{-13}	366.265	360.10	360.118	6.165	6.147
NGC 4473	0.90×10^8	15.25	2.815×10^{-13}	240.628	236.563	236.574	4.065	4.054
NGC 4459	6.96×10^7	16.01	2.073×10^{-13}	186.086	182.94	182.95	3.146	3.136
M32	2.45×10^6	0.8057	1.450×10^{-13}	6.5504	6.4397	6.44007	0.1107	0.1097

and $\alpha - \beta$ when Sgr A* is modelled as string-inspired Euler-Heisenberg BH at the value of angular shadow diameter $\theta_{sh} = 50 \mu as$ and $\theta_{sh} = 46.9 \mu as$. In Table. VI we estimate the parameters Q^2 and $\alpha - \beta$ when M87* is modelled as string-inspired Euler-Heisenberg BH at the value of angular shadow diameter $\theta_{sh} = 39 \mu as$. The analysis reveals that substantial variations in the parameter $\alpha - \beta$ do not significantly alter the angular shadow diameter (θ_{sh}).

$\theta_{sh} = 50 \mu as$		$\theta_{sh} = 46.9 \mu as$
$(\alpha - \beta)$	Q^2	Q^2
-1.75	0.28778	0.57651
-3.25	0.28373	0.55344
-4.75	0.27989	0.53304
-6.25	0.27623	0.51477
-7.75	0.27274	0.49824
-9.25	0.26941	0.48316

TABLE IV: Estimation of values of parameters Q^2 for different values of $(\alpha - \beta)$ corresponding to $\theta_{sh} = 50 \mu as$ and $\theta_{sh} = 46.9 \mu as$ for the string-inspired Euler-Heisenberg black holes as Sgr A*.

$\theta_{sh} = 50 \mu as$		$\theta_{sh} = 46.9 \mu as$	
Q^2	$(\alpha - \beta)$	Q^2	$(\alpha - \beta)$
0.265	-11.34	0.505	-7.12
0.270	-8.977	0.520	-5.805
0.275	-6.77	0.535	-4.598
0.280	-4.706	0.550	-3.491
0.285	-2.77	0.565	-2.474
0.290	-0.96	0.580	-1.539

TABLE V: Estimation of values of parameters $(\alpha - \beta)$ for different values of Q^2 corresponding to $\theta_{sh} = 50 \mu as$ and $\theta_{sh} = 46.9 \mu as$ for the string-inspired Euler-Heisenberg black holes as Sgr A*.

$\theta_{sh} = 39 \mu as$		$\theta_{sh} = 39 \mu as$	
$(\alpha - \beta)$	Q^2	Q^2	$(\alpha - \beta)$
-1.75	0.08439	0.0825	-12.1
-3.25	0.08411	0.0829	-9.8
-4.75	0.08391	0.0833	-7.6
-6.25	0.08355	0.0837	-5.4
-7.75	0.08327	0.0841	-3.3
-9.25	0.0830	0.0845	-1.2

TABLE VI: Estimation of values of parameters Q^2 and $(\alpha - \beta)$ for different values of $(\alpha - \beta)$ and Q^2 respectively corresponding to $\theta_{sh} = 39 \mu as$ for the string-inspired Euler-Heisenberg black holes as M87*.

VI. CONCLUSION

The study explores the influence of parameters Q^2 and $(\alpha - \beta)$ on gravitational lensing phenomena associated with string-inspired Euler-Heisenberg black holes, comparing them with the Schwarzschild black hole of General Relativity (GR). It reveals that the photon sphere radius x_{ps} contracts with increasing magnitude of Q^2 and $\alpha - \beta$, indicating smaller photon spheres in string-inspired Euler-Heisenberg black holes than GR. Furthermore, the critical impact parameter u_{ps} has a decreasing behaviour for Q^2 and $(\alpha - \beta)$, which is qualitatively similar to the behaviour of the unstable photon orbit radius x_{ps} . Its value is consistently lower than that of its GR equivalents. On the other hand, the strong-gravitational lensing coefficients \bar{a} tend to increase with Q^2 as well as $(\alpha - \beta)$ but \bar{b} tends to exhibit a gradual decrease with increasing magnitude of $(\alpha - \beta)$ and Q^2 . The deflection angle α_D , for a fixed impact parameter u , is smaller in string-inspired Euler-Heisenberg black holes than in Schwarzschild black holes, decreasing further with increasing Q^2 .

Further investigations focus on strong lensing observables for supermassive black holes, Sgr A* and M87*, under string-inspired Euler-Heisenberg black hole spacetime. The study finds that string-inspired Euler-Heisenberg black holes closely approximate GR predictions, with lensing observables such as θ_∞ , the separation s between images, and the magnification ratio r_{mag} showing ranges consistent with GR expectations. However, deviations from GR are observed, particularly in θ_∞ , which ranges between 23.81 - 26.28 μas for Sgr A* and 17.89 - 19.77 μas for M87*, with deviations as high as 2.452 μas and 1.89 μas , respectively.

Finally, the study evaluates the time delay of relativistic images in string-inspired Euler-Heisenberg black hole spacetime, finding them consistent with GR predictions.

For instance, the time delay for M87* is approximately ~ 293 minutes, while for Sgr A*, it's around ~ 0.19 minutes. Except for Sgr A*, these time delay differences are substantial enough for astronomical observations, assuming sufficient angular resolution exists between the two relativistic pictures. While string-inspired Euler-Heisenberg black holes exhibit deviations from GR predictions for certain lensing observables, they largely align with GR expectations, suggesting their potential as a valid description for astrophysical black hole phenomena.

The constraints derived from EHT observations indicate that string-inspired Euler-Heisenberg black holes may provide a viable description for the spacetime of astrophysical black holes within limited parameter ranges. Specifically, for M87*, Q^2 is constrained to $0.0 < Q^2 \leq 0.0847$, while for Sgr A*, it falls within $0.292 \leq Q^2 \leq 0.607$, at the 1σ confidence level. These constraints on Q^2 do not impose any limitations on the parameter $\alpha - \beta$. The parameter estimation conducted using the EHT data for the angular diameter shadow (θ_{sh}) of Sgr A* and M87* serves as a crucial validation step in affirming the viability of string-inspired Euler-Heisenberg black holes as astrophysical black hole candidates. While string-inspired Euler-Heisenberg black holes show promise in modelling black hole spacetime, further exploration of the full parameter space, particularly regarding $\alpha - \beta$, is warranted to understand their viability in astrophysical contexts comprehensively.

VII. ACKNOWLEDGMENTS

A.V and S.G.G. would like to thank SERB-DST for project No. CRG/2021/005771.

-
- [1] Akiyama K., et al. (Event Horizon Telescope), *Astrophys. J. Lett.*, 2019, **875**, L1, doi:10.3847/2041-8213/ab0ec7, 1906.11238.
 - [2] Akiyama K., et al. (Event Horizon Telescope), *Astrophys. J. Lett.*, 2022, **930**, No. 2, L12, doi:10.3847/2041-8213/ac6674, 2311.08680.
 - [3] Perlick V., 2010, 1010.3416.
 - [4] Einstein A., *Science*, 1936, **84**, 506–507, doi:10.1126/science.84.2188.506.
 - [5] Liebes S., *Phys. Rev.*, 1964, **133**, B835–B844, doi:10.1103/PhysRev.133.B835.
 - [6] Mellier Y., *Ann. Rev. Astron. Astrophys.*, 1999, **37**, 127–189, doi:10.1146/annurev.astro.37.1.127, astro-ph/9812172.
 - [7] Bartelmann M., Schneider P., *Phys. Rept.*, 2001, **340**, 291–472, doi:10.1016/S0370-1573(00)00082-X, astro-ph/9912508.
 - [8] Schmidt F., *Phys. Rev. D*, 2008, **78**, 043002, doi:10.1103/PhysRevD.78.043002, 0805.4812.
 - [9] Barnacka A., *Detection techniques for the H.E.S.S. II telescope, data modeling of gravitational lensing and emission of blazars in HE-VHE astronomy*, Other thesis, 2013, 1307.4050.
 - [10] C. Darwin, *The gravity field of a particle*, *Proc. R. Soc. Lond. A* 249, 180 (1959).
 - [11] Luminet J. P., *Astron. Astrophys.*, 1979, **75**, 228–235.
 - [12] Virbhadra K. S., Ellis G. F. R., *Phys. Rev. D*, 2000, **62**, 084003, doi:10.1103/PhysRevD.62.084003, astro-ph/9904193.
 - [13] Virbhadra K. S., Ellis G. F. R., *Phys. Rev. D*, 2002, **65**, 103004, doi:10.1103/PhysRevD.65.103004.
 - [14] Frittelli S., Kling T. P., Newman E. T., *Phys. Rev. D*, 2000, **61**, 064021, doi:10.1103/PhysRevD.61.064021, gr-qc/0001037.
 - [15] Bozza V., Capozziello S., Iovane G., Scarpetta G., *Gen. Rel. Grav.*, 2001, **33**, 1535–1548, doi:10.1023/A:1012292927358, gr-qc/0102068.
 - [16] Bozza V., *Phys. Rev. D*, 2002, **66**, 103001, doi:10.1103/PhysRevD.66.103001, gr-qc/0208075.
 - [17] Bozza V., Scarpetta G., *Phys. Rev. D*, 2007, **76**, 083008,

- doi:10.1103/PhysRevD.76.083008, 0705.0246.
- [18] Bozza V., *Phys. Rev. D*, 2003, **67**, 103006, doi:10.1103/PhysRevD.67.103006, gr-qc/0210109.
- [19] Tsukamoto N., *Phys. Rev. D*, 2017, **95**, No. 6, 064035, doi:10.1103/PhysRevD.95.064035, 1612.08251.
- [20] Tsukamoto N., *Phys. Rev. D*, 2018, **97**, No. 6, 064021, doi:10.1103/PhysRevD.97.064021, 1708.07427.
- [21] Eiroa E. F., Romero G. E., Torres D. F., *Phys. Rev. D*, 2002, **66**, 024010, doi:10.1103/PhysRevD.66.024010, gr-qc/0203049.
- [22] Bozza V., *Gen. Rel. Grav.*, 2010, **42**, 2269–2300, doi:10.1007/s10714-010-0988-2, 0911.2187.
- [23] Iyer S. V., Petters A. O., *Gen. Rel. Grav.*, 2007, **39**, 1563–1582, doi:10.1007/s10714-007-0481-8, gr-qc/0611086.
- [24] Virbhadra K. S., Keeton C. R., *Phys. Rev. D*, 2008, **77**, 124014, doi:10.1103/PhysRevD.77.124014, 0710.2333.
- [25] Shaikh R., Banerjee P., Paul S., Sarkar T., *JCAP*, 2019, **07**, 028, doi:10.1088/1475-7516/2019/07/028, [Erratum: *JCAP* 12, E01 (2023)], 1905.06932.
- [26] Ghosh S. G., Kumar R., Islam S. U., *JCAP*, 2021, **03**, 056, doi:10.1088/1475-7516/2021/03/056, 2011.08023.
- [27] Whisker R., *Phys. Rev. D*, 2005, **71**, 064004, doi:10.1103/PhysRevD.71.064004, astro-ph/0411786.
- [28] Abbas G., Mahmood A., Zubair M., *Phys. Dark Univ.*, 2021, **31**, 100750, doi:10.1016/j.dark.2020.100750.
- [29] Eiroa E. F., *Phys. Rev. D*, 2006, **73**, 043002, doi:10.1103/PhysRevD.73.043002, gr-qc/0511065.
- [30] Gylchev G. N., Yazadjiev S. S., *Phys. Rev. D*, 2007, **75**, 023006, doi:10.1103/PhysRevD.75.023006, gr-qc/0611110.
- [31] Ghosh T., Sengupta S., *Phys. Rev. D*, 2010, **81**, 044013, doi:10.1103/PhysRevD.81.044013, 1001.5129.
- [32] Gylchev G. N., Stefanov I. Z., *Phys. Rev. D*, 2013, **87**, No. 6, 063005, doi:10.1103/PhysRevD.87.063005, 1211.3458.
- [33] Molla N. U., Ali A., Debnath U., 2023, 2307.11798.
- [34] Grespan M., Biesiada M., *Universe*, 2023, **9**, No. 5, 200, doi:10.3390/universe9050200.
- [35] Kumar J., Islam S. U., Ghosh S. G., *Astrophys. J.*, 2022, **938**, No. 2, 104, doi:10.3847/1538-4357/ac912c, 2209.04240.
- [36] Kumar Walia R., *JCAP*, 2023, **03**, 029, doi:10.1088/1475-7516/2023/03/029, 2207.02106.
- [37] Kumar J., Islam S. U., Ghosh S. G., *Eur. Phys. J. C*, 2022, **82**, No. 5, 443, doi:10.1140/epjc/s10052-022-10357-2, 2109.04450.
- [38] Lu X., Xie Y., *Eur. Phys. J. C*, 2021, **81**, No. 7, 627, doi:10.1140/epjc/s10052-021-09440-x.
- [39] Ali M. S., Kauhsal S., *Phys. Rev. D*, 2022, **105**, No. 2, 024062, doi:10.1103/PhysRevD.105.024062, 2106.08464.
- [40] Hsieh T., Lee D.-S., Lin C.-Y., *Phys. Rev. D*, 2021, **103**, No. 10, 104063, doi:10.1103/PhysRevD.103.104063, 2101.09008.
- [41] Chen S.-b., Jing J.-l., *Phys. Rev. D*, 2009, **80**, 024036, doi:10.1103/PhysRevD.80.024036, 0905.2055.
- [42] Sarkar K., Bhadra A., *Class. Quant. Grav.*, 2006, **23**, 6101–6113, doi:10.1088/0264-9381/23/22/002, gr-qc/0602087.
- [43] Javed W., Babar R., Övgün A., *Phys. Rev. D*, 2019, **99**, No. 8, 084012, doi:10.1103/PhysRevD.99.084012, 1903.11657.
- [44] Shaikh R., Banerjee P., Paul S., Sarkar T., *Phys. Rev. D*, 2019, **99**, No. 10, 104040, doi:10.1103/PhysRevD.99.104040, 1903.08211.
- [45] Eiroa E. F., Sendra C. M., *Class. Quant. Grav.*, 2011, **28**, 085008, doi:10.1088/0264-9381/28/8/085008, 1011.2455.
- [46] Övgün A., *Phys. Rev. D*, 2019, **99**, No. 10, 104075, doi:10.1103/PhysRevD.99.104075, 1902.04411.
- [47] Panpanich S., Ponglertsakul S., Tannukij L., *Phys. Rev. D*, 2019, **100**, No. 4, 044031, doi:10.1103/PhysRevD.100.044031, 1904.02915.
- [48] Bronnikov K. A., Baleevskikh K. A., *Grav. Cosmol.*, 2019, **25**, No. 1, 44–49, doi:10.1134/S020228931901002X, 1812.05704.
- [49] Shaikh R., Banerjee P., Paul S., Sarkar T., *Phys. Lett. B*, 2019, **789**, 270–275, doi:10.1016/j.physletb.2018.12.030, [Erratum: *Phys.Lett.B* 791, 422–423 (2019)], 1811.08245.
- [50] Babar G. Z., Atamurotov F., Ul Islam S., Ghosh S. G., *Phys. Rev. D*, 2021, **103**, No. 8, 084057, doi:10.1103/PhysRevD.103.084057, 2104.00714.
- [51] Kumar R., Islam S. U., Ghosh S. G., *Eur. Phys. J. C*, 2020, **80**, No. 12, 1128, doi:10.1140/epjc/s10052-020-08606-3, 2004.12970.
- [52] Islam S. U., Kumar R., Ghosh S. G., *JCAP*, 2020, **09**, 030, doi:10.1088/1475-7516/2020/09/030, 2004.01038.
- [53] Narzilloev B., Shaymatov S., Hussain I., Abdujabbarov A., Ahmedov B., Bambi C., *Eur. Phys. J. C*, 2021, **81**, 849, doi:10.1140/epjc/s10052-021-09617-4, 2109.02816.
- [54] Sygne J. L., *Mon. Not. Roy. Astron. Soc.*, 1966, **131**, No. 3, 463–466, doi:10.1093/mnras/131.3.463.
- [55] Gralla S. E., Holz D. E., Wald R. M., *Phys. Rev. D*, 2019, **100**, No. 2, 024018, doi:10.1103/PhysRevD.100.024018, 1906.00873.
- [56] Darwin C. G., *Proceedings of the Royal Society of London. Series A. Mathematical and Physical Sciences*, 1959, **249**, No. 1257, 180–194.
- [57] Cunha P. V. P., Herdeiro C. A. R., *Gen. Rel. Grav.*, 2018, **50**, No. 4, 42, doi:10.1007/s10714-018-2361-9, 1801.00860.
- [58] Gibbons G. W., Maeda K.-i., *Nucl. Phys. B*, 1988, **298**, 741–775, doi:10.1016/0550-3213(88)90006-5.
- [59] Garfinkle D., Horowitz G. T., Strominger A., *Phys. Rev. D*, 1991, **43**, 3140, doi:10.1103/PhysRevD.43.3140, [Erratum: *Phys.Rev.D* 45, 3888 (1992)].
- [60] Bhadra A., *Phys. Rev. D*, 2003, **67**, 103009, doi:10.1103/PhysRevD.67.103009, gr-qc/0306016.
- [61] Sharif M., Iftikhar S., *Soviet Journal of Experimental and Theoretical Physics*, 2017, **124**, No. 6, 886–894, doi:10.1134/S1063776117050065.
- [62] Younesizadeh Y., Younesizadeh F., Qaemmaqami M. M., *Eur. Phys. J. Plus*, 2022, **137**, No. 1, 76, doi:10.1140/epjp/s13360-021-02290-2, 2206.05456.
- [63] Molla N. U., Ghosh S. G., Debnath U., *Phys. Dark Univ.*, 2024, **44**, 101495, doi:10.1016/j.dark.2024.101495.
- [64] Cano P. A., Chimento S., Linares R., Ortiin T., Ramirez P. F., *Journal of High Energy Physics*, 2020, **2020**, No. 2, 1–31.
- [65] Bakopoulos A., Karakasis T., Mavromatos N. E., Nakas T., Papantonopoulos E., 2024, 2402.12459.
- [66] Charmousis C., Gouteraux B., Kiritsis E., *JHEP*, 2012, **09**, 011, doi:10.1007/JHEP09(2012)011, 1206.1499.
- [67] Gross D. J., Sloan J. H., *Nucl. Phys. B*, 1987, **291**, 41–89, doi:10.1016/0550-3213(87)90465-2.
- [68] Green M. B., Schwarz J. H., Witten E., *Superstring Theory Vol. 1: 25th Anniversary Edition*, Cambridge Mono-

- graphs on Mathematical Physics, Cambridge University Press, 2012, doi:10.1017/CBO9781139248563.
- [69] Green M. B., Schwarz J. H., Witten E., *Superstring Theory Vol. 2: 25th Anniversary Edition*, Cambridge Monographs on Mathematical Physics, Cambridge University Press, 2012, doi:10.1017/CBO9781139248570.
- [70] Schwarzschild K., *Sitzungsberichte der Königlich Preussischen Akademie der Wissenschaften*, 1916, 189–196.
- [71] Pugliese D., Quevedo H., Ruffini R., *Phys. Rev. D*, 2011, **83**, 024021, doi:10.1103/PhysRevD.83.024021, 1012.5411.
- [72] Claudel C.-M., Virbhadra K. S., Ellis G. F. R., *J. Math. Phys.*, 2001, **42**, 818–838, doi:10.1063/1.1308507, gr-qc/0005050.
- [73] Jha S. K., Rahaman A., *Eur. Phys. J. Plus*, 2023, **138**, No. 1, 86, doi:10.1140/epjp/s13360-023-03650-w.
- [74] Islam S. U., Ghosh S. G., *Phys. Rev. D*, 2021, **103**, No. 12, 124052, doi:10.1103/PhysRevD.103.124052, 2102.08289.
- [75] Bozza V., Mancini L., *Gen. Rel. Grav.*, 2004, **36**, 435–450, doi:10.1023/B:GERG.0000010486.58026.4f, gr-qc/0305007.
- [76] Virbhadra K. S., Narasimha D., Chitre S. M., *Astron. Astrophys.*, 1998, **337**, 1–8, astro-ph/9801174.
- [77] Akiyama K., et al. (Event Horizon Telescope), *Astrophys. J. Lett.*, 2019, **875**, No. 1, L6, doi:10.3847/2041-8213/ab1141, 1906.11243.
- [78] Chen Z., et al., *Astrophys. J. Lett.*, 2019, **882**, No. 2, L28, doi:10.3847/2041-8213/ab3c68, 1908.08066.
- [79] Bozza V., Mancini L., *Astrophys. J.*, 2004, **611**, 1045–1053, doi:10.1086/422309, astro-ph/0404526.
- [80] Akiyama K., et al. (Event Horizon Telescope), *Astrophys. J. Lett.*, 2019, **875**, No. 1, L5, doi:10.3847/2041-8213/ab0f43, 1906.11242.
- [81] Akiyama K., et al. (Event Horizon Telescope), *Astrophys. J. Lett.*, 2022, **930**, No. 2, L17, doi:10.3847/2041-8213/ac6756, 2311.09484.
- [82] Afrin M., Ghosh S. G., *Astrophys. J.*, 2022, **932**, No. 1, 51, doi:10.3847/1538-4357/ac6dda, 2110.05258.
- [83] Zakharov A. F., *Universe*, 2022, **8**, No. 3, 141, doi:10.3390/universe8030141, 2108.01533.
- [84] Kocherlakota P., et al. (Event Horizon Telescope), *Phys. Rev. D*, 2021, **103**, No. 10, 104047, doi:10.1103/PhysRevD.103.104047, 2105.09343.
- [85] Kumar R., Ghosh S. G., *Astrophys. J.*, 2020, **892**, 78, doi:10.3847/1538-4357/ab77b0, 1811.01260.
- [86] Kumar Walia R., Ghosh S. G., Maharaj S. D., *Astrophys. J.*, 2022, **939**, No. 2, 77, doi:10.3847/1538-4357/ac9623, 2207.00078.
- [87] Ghosh S. G., Afrin M., *Astrophys. J.*, 2023, **944**, No. 2, 174, doi:10.3847/1538-4357/acb695, 2206.02488.
- [88] Kumar J., Islam S. U., Ghosh S. G., *Eur. Phys. J. C*, 2023, **83**, No. 11, 1014, doi:10.1140/epjc/s10052-023-12205-3, 2305.04336.
- [89] Islam S. U., Kumar J., Kumar Walia R., Ghosh S. G., *Astrophys. J.*, 2023, **943**, No. 1, 22, doi:10.3847/1538-4357/aca411, 2211.06653.
- [90] Kumar J., Islam S. U., Ghosh S. G., *JCAP*, 2022, **11**, 032, doi:10.1088/1475-7516/2022/11/032, 2209.13562.
- [91] Tsukamoto N., *Phys. Rev. D*, 2021, **103**, No. 2, 024033, doi:10.1103/PhysRevD.103.024033, 2011.03932.